ACS OMEGA

http://pubs.acs.org/journal/acsodf

Article

Prediction Method of Coal Texture Considering Longitudinal Resolution of Logging Curves and Its Application—Taking No. 15 Coal Seam in the Shouyang Block as an Example

Shouren Zhang,* Xinyang Men, Zhiyu Deng, and Qiuping Hu

Cite This: *ACS Omega* 2023, 8, 28702−28714

Read Online

ACCESS | Metrics & More | Article Recommendations

ABSTRACT: The quantitative identification of the coal texture is of great importance as a crucial parameter for coalbed methane (CBM) reservoir evaluation. This study combined drilling core data, electrical imaging logging data, and four conventional logging data, namely, compensation density (DEN), natural γ (GR), deep lateral resistivity (RD), and acoustic time difference (AC), to achieve accurate inversion of coal texture in the Shouyang Block. Meanwhile, wavelet analysis and Fisher discriminant analysis were introduced to the inversion process to further improve the accuracy. Through the utilization of software packages, such as Matlab and SPSS, the establishment of the coal texture logging interpretation chart of the No. 15 coal seam in the Shouyang block was successfully realized. The outcome of this comprehensive study reveals that the coal texture logging interpretation chart is an effective tool for the identification and classification of each coal texture and gangue. Moreover, the validity and reliability of this method were tested and confirmed using wells CS-8 and CS-9 in the region, achieving an accuracy of 97.1 and 93.2%, respectively. This innovative method has significant prospects for predicting and evaluating the coal texture in the Shouyang Block, which can be further applied to other regions.

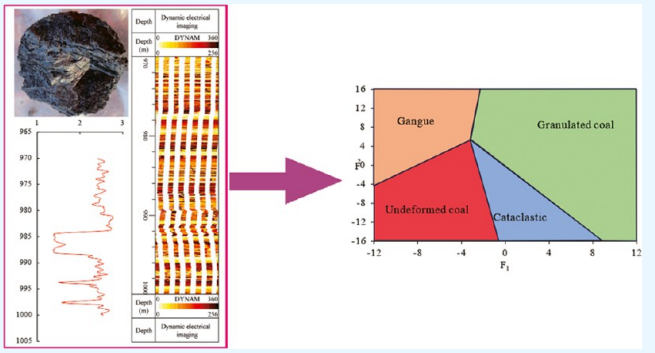

INTRODUCTION

Coal texture refers to the structural characteristics of coal seams that have undergone various geological processes during the geological evolution process. Due to the low Young's modulus and high Poisson's ratio of coal, the coal seam is prone to deformation, damage, crushing, and rheology, forming different coal textures.[1] Coal texture, as an observable manifestation of the degree of structural deformation, significantly influences the physical characteristics of the coal reservoirs, the selection of fracturing layers, and the development outcomes. Consequently, it serves as a crucial indicator for evaluating coalbed methane reservoirs.[2,3] The No. 3 coal seam of Shanxi Formation and the No. 15 coal seam of Taiyuan Formation are the main coal seams for coalbed methane development in the Shouyang Block. The coal texture of these coal seams is complex, variable, and unstable in distribution. Therefore, it is urgent to establish an effective method for distinguishing coal texture. Logging curves, as an indirect parameter for identifying coal texture, have applicability advantages compared to identifying coal texture with coal cores, which may be affected by drilling and lead to misjudgment.[4] Early research on coal texture prediction based on logging curves primarily employed cluster analysis[5] and the Protodyakonov's coefficient method.[6] Subsequently, methods such as Archie's formula,[7] coal texture index,[8] brittleness index,[9] geological strength index (GSI),[10] K-means algorithm,[11] principal component analysis,[12] neural network,[13,14] Fisher discriminant analysis,[15] and other quantitative classification techniques were gradually introduced. Although many logging interpretation models for coal texture have already been built, there are still some shortcomings in coal texture correction and interpretation accuracy. Moreover, there is still a lack of effective identification of gangues in complex coal seams. Thus, in this study, the No. 15 coal seam in the Shouyang Block was selected as the research object to tackle this challenge. To improve the accuracy of coal texture classification, core correction was performed by electrical imaging logging data.[16] Furthermore, the wavelet analysis method was used to decompose and reconstruct the logging curve and improve its longitudinal resolution. Finally, a coal texture logging interpretation chart was built to distinguish different coal textures and gangue. This

Received: May 16, 2023
Accepted: July 17, 2023
Published: July 25, 2023

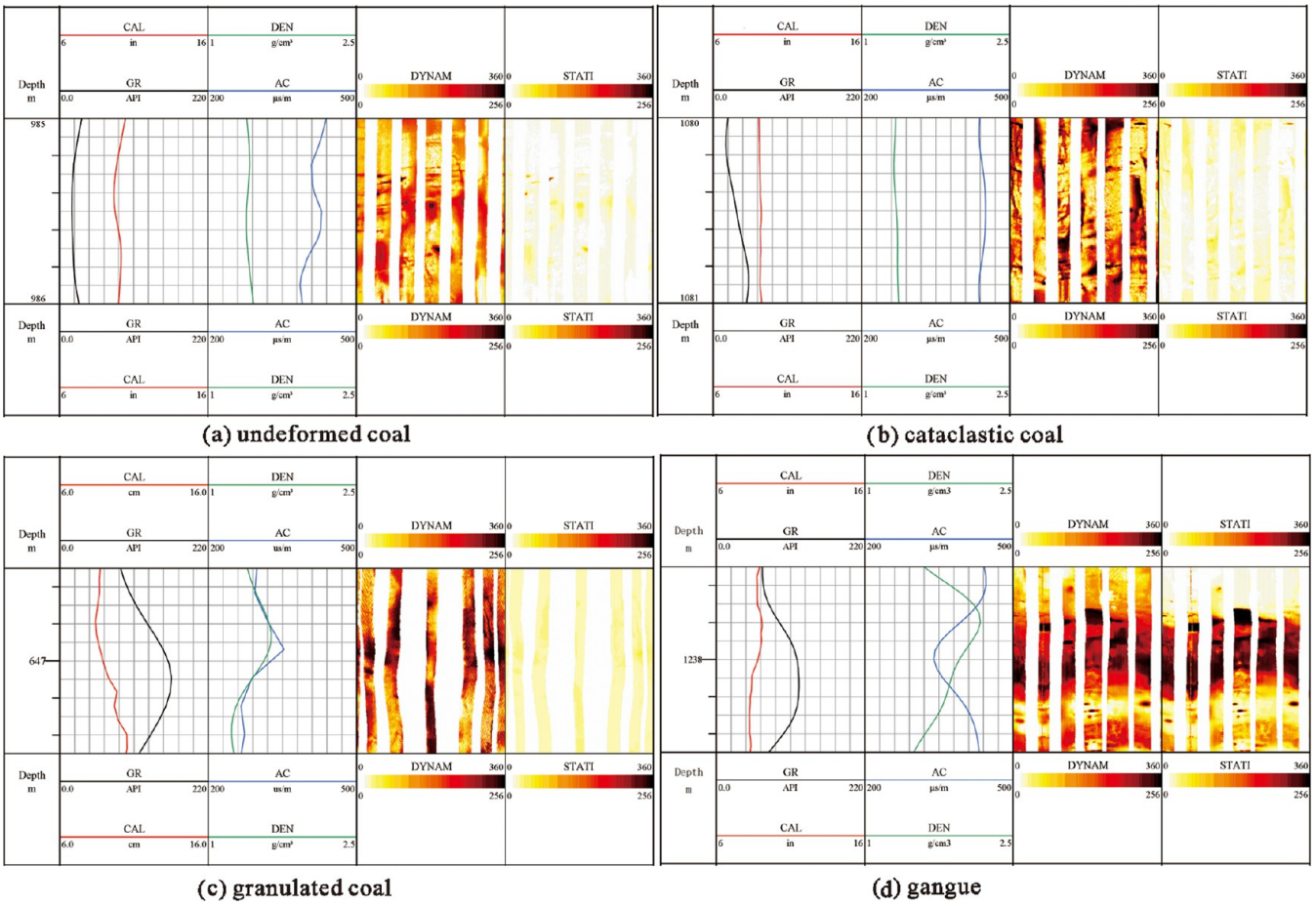

Figure 1. Electrical imaging recognition patterns of coal textures in the Shouyang Block.

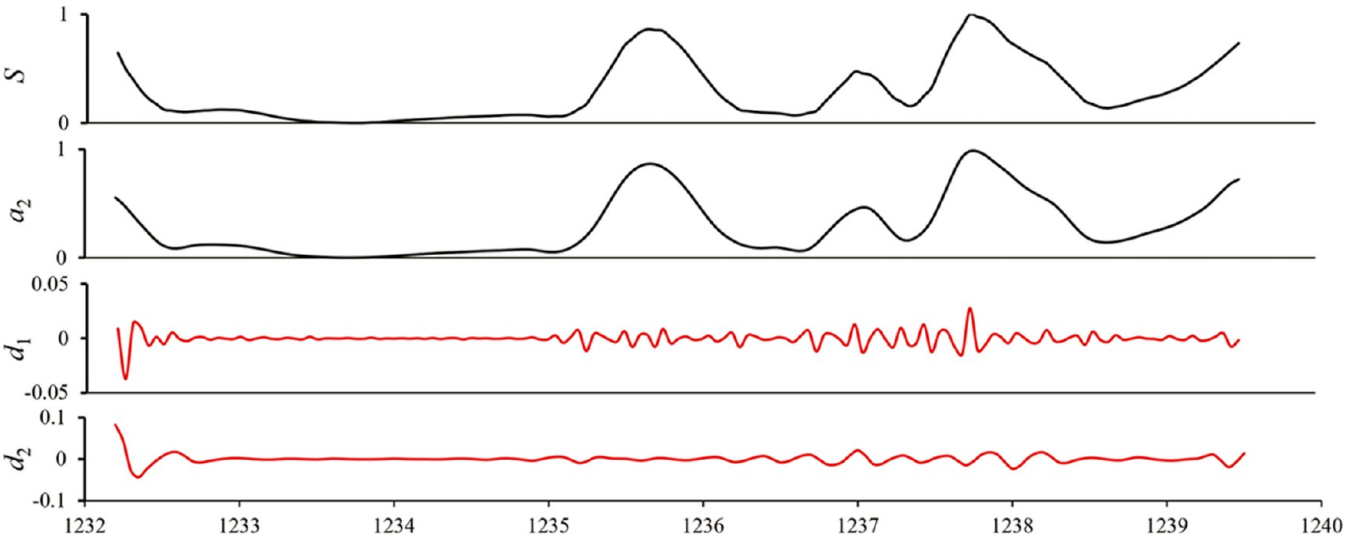

Figure 2. Schematic diagram of wavelet decomposition of the compensated density logging curve.

model has the advantages of high recognition accuracy and the ability to identify gangues in complex coal seams.

ESTABLISHMENT OF A LOGGING INTERPRETATION CHART FOR COAL TEXTURE

Core Repositioning and Coal Texture Correction by Electrical Imaging Logging. Logging interpretation of coal texture requires establishing a corresponding relationship between logging parameters and coal cores. Nonetheless, due to the influence of drilling tools and environmental factors, the coring depth needs to be meticulously corrected to match the logging depth. The core repositioning is accomplished by formula 1

$$D' = D_2' - (D_2 - D) \times \frac{h'}{h} \quad (1)$$

https://doi.org/10.1021/acsomega.3c03399
ACS Omega 2023, 8, 28702−28714

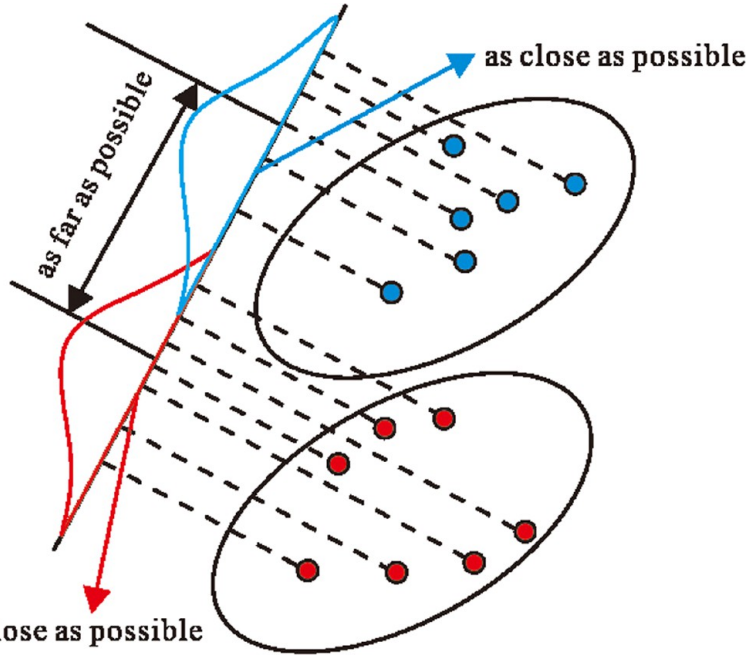

Figure 3. Schematic diagram of Fisher discriminant analysis. Reprinted (adapted or reprinted in part) with permission from Chen et al.[15] Identification of thin-layer coal texture using geophysical logging data: Investigation by wavelet transform and linear discrimination analysis. Copyright [2021] [Elsevier].

where h and h' are the coal seam thicknesses obtained from drilling and logging interpretation, respectively, m; D_1 and D_2 are the top and bottom depths obtained from drilling, respectively, m; D_1' and D_2' are the top and bottom depths of the coal seam obtained from logging interpretation, respectively, m; D and D' are the coal sample depths obtained from drilling and logging interpretation, respectively, m.

During the conventional coring process, coal texture is often plagued by issues, such as broken cores and distorted coal textures, due to drilling fluid, stress release, and other factors. The visual characteristics of electrical imaging logging can provide a solution by compensating for these deficiencies and enhancing the accuracy of coal texture classification. The national standard GB/T 30050-2013 classifies coal textures into four categories: undeformed coal, cataclastic coal, granulated coal, and mylonitized coal, with the latter two often grouped together as structural coal or replaced directly with granulated coal during coalbed methane exploration and development.[17−21]

The images generated by processing the electrical imaging logging data are calibrated using a combination of static and dynamic color calibration methods.[22] The static color calibration employs a consistent color scheme across the entire wellbore, which reflects the relative changes in electrical resistivity throughout the wellbore, resulting in high discriminative power for lithological differentiation. For example, coal exhibits bright white color on the static image due to its high electrical resistance. The dynamic color calibration is used to address the conflict between limited color scales and the large range of resistivity changes across the entire wellbore. Generally, a color is assigned to each half-meter section for detailed stratigraphic analysis. In this study, a dynamic color recognition mode was established for the classification of coal textures, as shown in Figure 1. The corresponding classification is as follows: undeformed coal has an intact macroscopic structure, presenting a blocky or layered structure with a uniform yellow−red color on the electrical image; cataclastic coal has local development of external fissures, appearing as a blocky-layered structure with a yellow−brown color on the electrical image; granulated coal has a large number of external fissures, appearing as brown−yellow−black on the electrical image; and the gangue is characterized by low electrical resistance, resulting in dark black stripes on the electrical image.

Wavelet Transform. The logging data at a certain depth is a comprehensive result of the rock information within the detection range of the probe at that position.[23] In practical logging operations, there may be "boundary effects".[24] For example, a thin layer of high radioactivity sandwiched between two thick low-radioactivity layers may cause the GR value of the high radioactivity layer to be underestimated. Due to the common occurrence of mudstone and other gangue interlayers within coal seams, abrupt changes in rock properties can lead to distorted logging data and seriously affect the logging curves near the interlayer.

Currently, common signal processing techniques used to address "boundary effects" include the Walsh transform,[25] Fourier transform,[26] deconvolution,[27] and wavelet transform.[28] The wavelet transform, as a time−frequency analysis method for digital signals, has been widely applied in geophysical exploration and well logging analysis. Its mathematical expression for wavelet basis functions is

$$\psi(t)_{a,\tau} = \frac{1}{\sqrt{a}}\psi\left(\frac{t-\tau}{a}\right)(a > 0, \tau \in R) \quad (2)$$

where the parameter a is the scaling factor or scale factor, which characterizes the width and amplitude change of the wavelet function, and the parameter τ is the translation factor or time shift factor, which characterizes the shift position of the wavelet function on the time axis.

The wavelet toolbox in Matlab software was used to perform a 1D discrete wavelet transform on the logging data. Taking the two-level wavelet decomposition as an example, the original well

https://doi.org/10.1021/acsomega.3c03399
ACS Omega 2023, 8, 28702−28714

Table 1. Electrical Imaging Correction of Coal Texture of the No. 15 Coal Seam in the Shouyang Block (Taking CS-6 and CS-7 Wells as Examples)

Well name	Coal texture identification (uncorrected)	Coal texture identification (corrected)
SY-P17X1	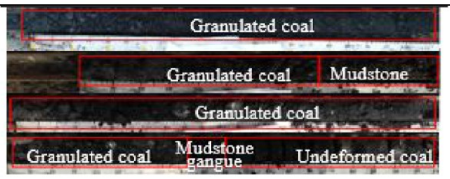	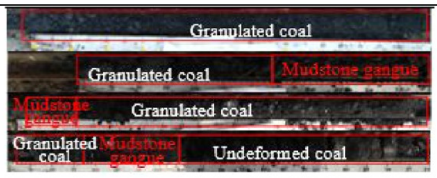
SY-P17X1		
SYE-26	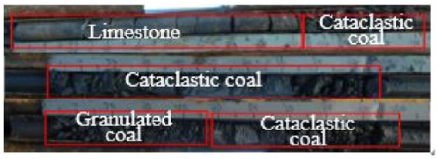	
SYE-26		

logging curve is divided into high-frequency wavelet coefficients (detail coefficients) and low-frequency wavelet coefficients (approximation coefficients) by high-pass and low-pass filters. Then, the SymN wavelet is used for two-level decomposition, and the first-level low-frequency wavelet coefficients are further decomposed into the second-level high-frequency wavelet coefficients and low-frequency wavelet coefficients (Figure 2). Wavelet reconstruction is the inverse process of wavelet decomposition, and the original well logging curve can be reconstructed from the decomposed signal using the following formula

$$s = a_1 + d_1 = a_2 + d_2 + d_1 \tag{3}$$

where s represents the original well logging curve; a_1 and a_2 represent the low-frequency wavelet coefficients after the first and second decomposition, respectively; d_1 and d_2 represent the high-frequency wavelet coefficients after the first and second decomposition, respectively.

Fisher Discriminant Analysis. Differences in coal pore and fracture development reflect in logging signals for different coal textures.[29−31] However, changes in coal texture are not abrupt, and although logging curves show certain trends with coal texture, there is an overlap in numerical values, which affects coal texture identification. To reduce the impact of overlap, a set of optimal discriminant vectors is determined based on Fisher discriminant analysis, which serves as the discriminating feature set for samples. The physical meaning of this feature set is that the pattern samples are projected onto these optimal discriminant vectors, and samples of the same class are concentrated, while samples of different classes are separated, such that the ratio of interclass scatter to intraclass scatter is maximized (Figure 3).

For an unknown sample set, it can also be classified by its distance or variance from known samples, ensuring high discrimination accuracy. The method is as follows.

A set of N d-dimensional samples $x_1, x_2, \cdots, x_n$, which belong to two different classes, i.e., there are N_1 samples belonging to the sample subset X_1 of class w_1 and N_2 samples belonging to the sample subset X_2 of class w_2. Define the intraclass scatter matrix S_w and interclass scatter matrix S_b of the samples, respectively

$$S_w = \sum_{i=1}^{2} \sum_{X \in X_i} (x - m_i)(x - m_i)^T \tag{4}$$

$$S_b = (m_1 - m_2)(m_1 - m_2)^T \tag{5}$$

where $m_i = \frac{1}{N_i} \sum_{X \in X_i} x$, $(i = 1, 2)$ m_i is the class mean. The intraclass scattering matrix S_w is a symmetric semipositive definite matrix and S_w is usually nonsingular when $N > d$. The interclass scattering matrix S_b is also a symmetric semipositive definite matrix and its rank is at most 1 since S_b is actually the outer product of two vectors.

The Fisher linear separability criterion requires maximizing the Fisher criterion function, i.e., finding a projection vector that maximizes the separation of the projected samples. The Fisher criterion function can be expressed as

$$J(w) = \frac{w^T S_b w}{w^T S_w w} \tag{6}$$

This expression is often referred to as the generalized Rayleigh quotient. The Lagrange multiplier method can be used to find w, such that $J(w)$ takes a great value. Let the denominator be a nonzero constant, i.e., let $w^T S_w w = c \neq 0$, and define the Lagrange function as

$$L(w, \lambda) = w^T S_b w - \lambda(w^T S_w w - c) \tag{7}$$

where λ is the Lagrange multiplier, and the partial derivative of w yields

https://doi.org/10.1021/acsomega.3c03399
ACS Omega 2023, 8, 28702−28714

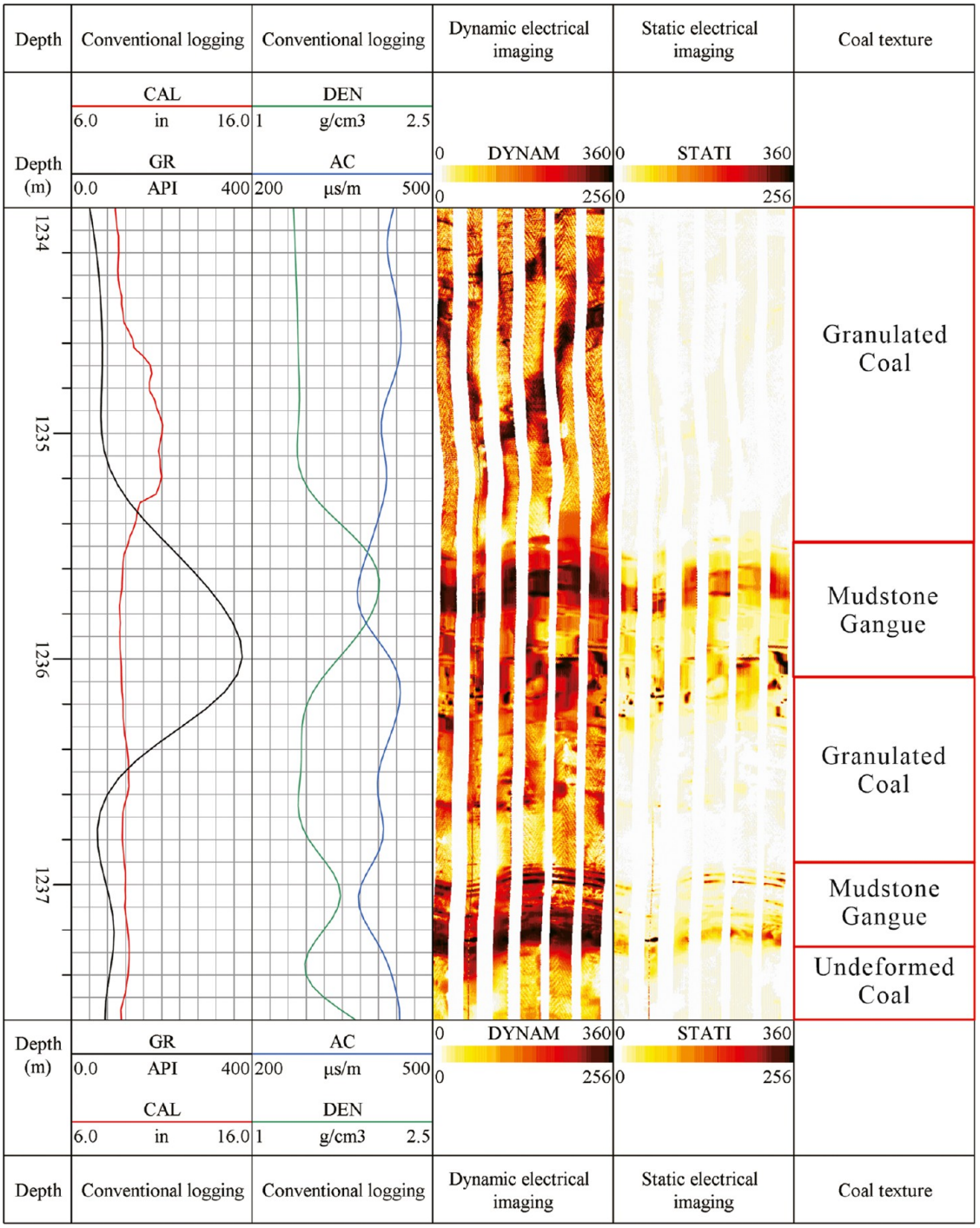

Figure 4. Electrical imaging identification map of coal texture in well CS-6 (the depth is 1234−1237.6 m).

$$\frac{\partial L(w, \lambda)}{\partial w} = S_b w - \lambda S_w w \tag{8}$$

Letting the partial derivative be zero, we have

$$S_b w - \lambda S_w w = 0 \tag{9}$$

If S_w is nonsingular, left multiplication of both sides by S_w^{-1} yields

$$S_w^{-1} S_b w = \lambda w \tag{10}$$

Equation 10 is the eigenvalue of the general matrix $S_w^{-1}S_b$. For binary classification problem, there is no need to truly calculate the eigenvalues of matrix $S_w^{-1}S_b$. Substituting eq 5 into the above equation yields

$$S_w^{-1}(m_1 - m_2)(m_1 - m_2)^T w = \lambda w \tag{11}$$

Since $(m_1 - m_2)^T w$ is a scalar quantity, let it be α, we get

$$w = \frac{\alpha}{\lambda} S_w^{-1}(m_1 - m_2) \tag{12}$$

where α/λ is a scalar factor that does not change the direction of the axis and is made to be 1. Then, we have

$$w = S_w^{-1}(m_1 - m_2) \tag{13}$$

https://doi.org/10.1021/acsomega.3c03399
ACS Omega 2023, 8, 28702−28714

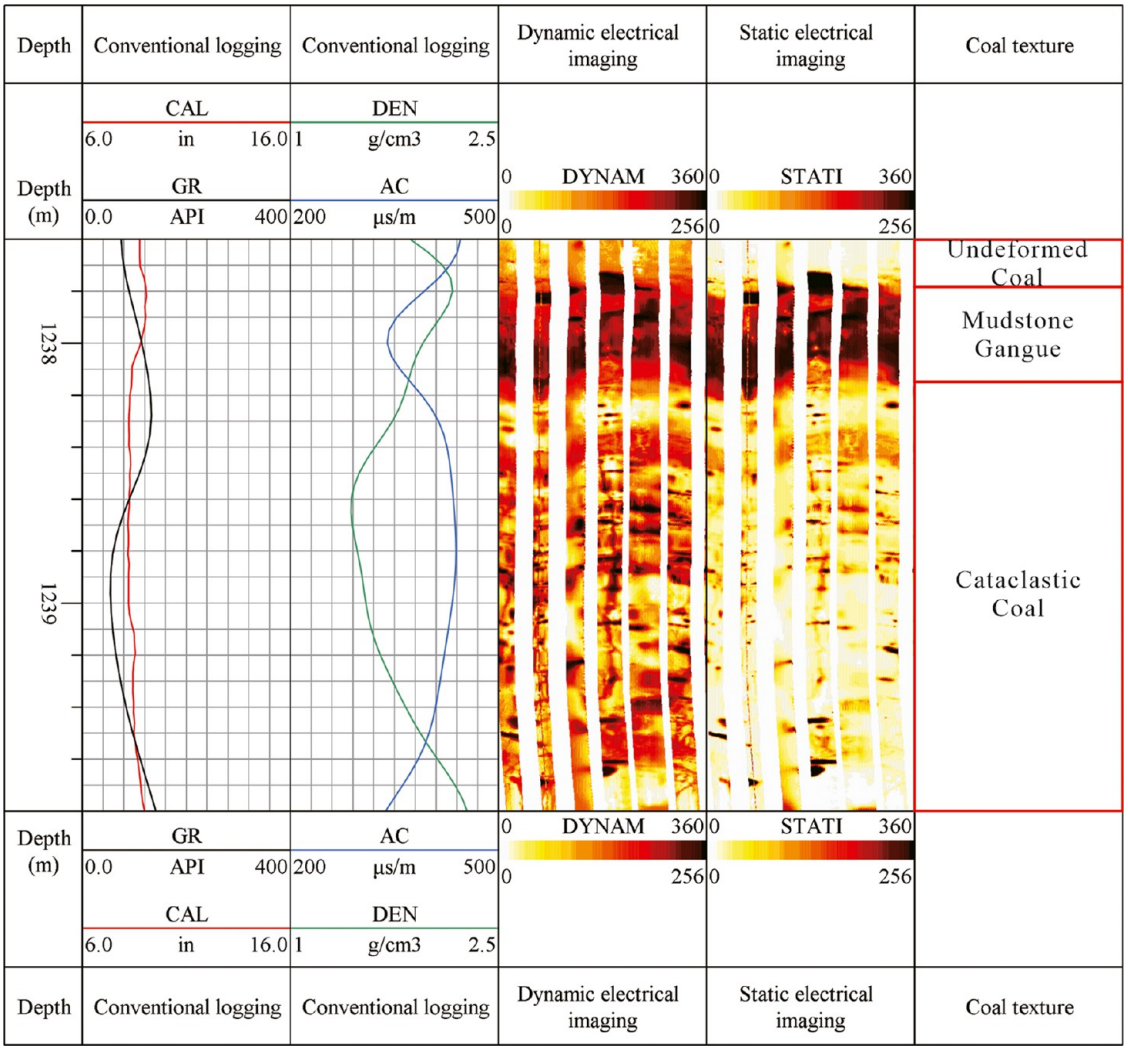

Figure 5. Electrical imaging identification map of coal texture in well CS-6 (the depth is 1237.6−1239.8 m).

The w obtained from eq 13 allows the Fisher criterion function $J(w)$ to take a great value, which is the best projection direction from the d-dimensional space to the one-dimensional space.

PRACTICAL APPLICATION IN THE SHOUYANG BLOCK

Coal Texture Correction. Coal core photos of seven wells, CS-1, CS-2, CS-3, CS-4,CS-5, CS-6, and CS-7, were used to identify and correct the coal texture. Some of the findings are presented in Table 1 and Figures 4−7. Electrical imaging logging images were used to accurately restore the fractured coal core to its original position and to identify the coal texture. Additionally, the gangue in the coal seam can also be identified.

Coal Texture Logging Interpretation Chart Establishment. Compensated density (DEN), natural γ (GR), deep lateral resistivity (RD), and acoustic time difference (AC) were used as the source data for the coal texture logging interpretation chart based on the characteristics of these logging curves. After normalization preprocessing, Sym8 wavelet was used for three-level decomposition of the DEN and GR curves, and Sym6 wavelet was used for four-level decomposition of the AC and RD curves based on the wavelet analysis toolbox in Matlab. The formula is as follows

$$s' = k_1 \times d_1 + k_2 \times d_2 + k_3 \times d_3 + k_3' \times a_3 \quad (14)$$

$$s' = k_1 \times d_1 + k_2 \times d_2 + k_3 \times d_3 + k_4 \times d_4 + k_4' \times a_4 \quad (15)$$

where s' represents the reconstructed logging curve; k_i and k_i' are the high-frequency and low-frequency wavelet compensation coefficients for the i-th level, respectively; and d_i and a_i represent the high-frequency and low-frequency wavelet coefficients for the i-th level, respectively.

As the noise decreases with the increasing decomposition level,[32] the first-level high-frequency wavelet coefficients with high noise content are removed. Meanwhile, the highest level high-frequency wavelet coefficients that exhibit the original curve style are compensated to highlight the curve amplitude and retain other levels of high-frequency wavelet coefficients. The improved formulas are as follows

$$s' = d_2 + k \times d_3 + a_3 \quad (16)$$

$$s' = d_2 + d_3 + k \times d_4 + a_4 \quad (17)$$

Taking the DEN curve as an example, appropriate high-frequency wavelet compensation coefficients are selected for reconstruction (Figure 8), which increases the curve amplitude while preserving the original curve shape. In this study, $k = 3$ is

https://doi.org/10.1021/acsomega.3c03399
ACS Omega 2023, 8, 28702−28714

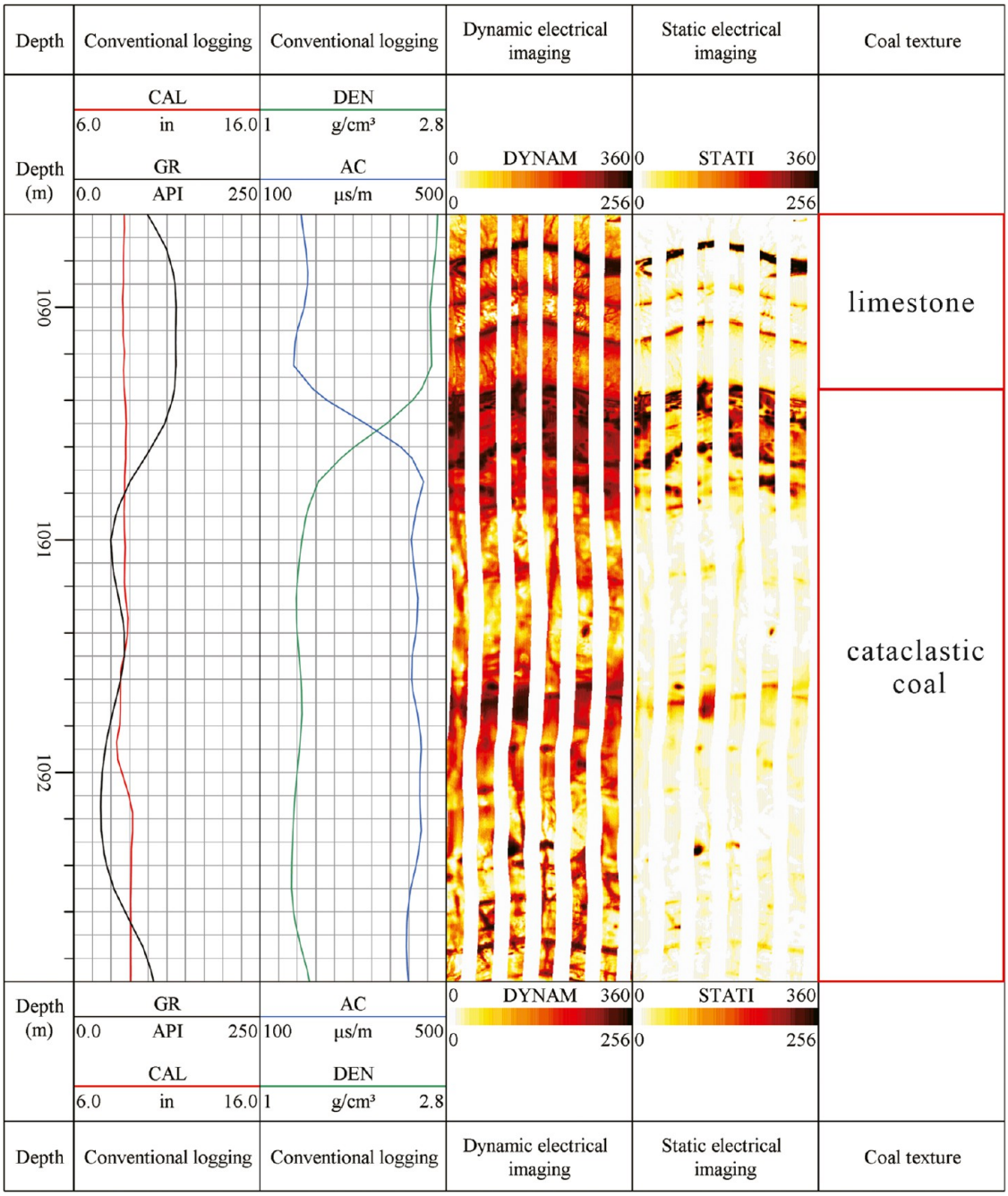

Figure 6. Electrical imaging identification map of coal texture in well CS-7 (the depth is 1089.6−1092.9 m).

selected as the compensation coefficient for the RD curve, $k = 4$ is selected as the compensation coefficient for the DEN and AC curves, and $k = 7$ is selected as the compensation coefficient for the GR curve (Figure 9). The overall trend of the curves corresponds well to the original signal curves, and the curve amplitudes are increased, effectively improving the logging vertical resolution.

For the reconstructed curves, 176 sampling points were extracted from the undeformed coal, cataclastic coal, granulated coal, and interbedded gangue at a sampling interval of 0.05 m to serve as data samples for the coal texture logging interpretation chart. Based on Fisher discriminant analysis, different coal texture logging data sample sets were assigned values (Table 2). The logging curves were used as the composition parameters of the vector matrix. SPSS software was used to perform Fisher discriminant analysis on the independent variables of undeformed coal, cataclastic coal, granulated coal, and gangue, respectively, to obtain the nonstandardized discrimination coefficients and discrimination functions (Table 3). The results are as follows

$$F_1 = 4.3203 \times \mathrm{DEN} + 0.0104 \times \mathrm{AC} - 0.0068 \times \mathrm{GR} + 0.0034 \times \mathrm{RD} - 18.3341 \quad (18)$$

$$F_2 = 18.7134 \times \mathrm{DEN} + 0.0200 \times \mathrm{AC} + 0.0154 \times \mathrm{GR} + 0.0010 \times \mathrm{RD} - 38.3838 \quad (19)$$

The characteristic values of typical discrimination functions are shown in Table 4. The characteristic value of F_1 is 23.149, with a variance of 64.3% and a typical correlation of 0.979. The

https://doi.org/10.1021/acsomega.3c03399
ACS Omega 2023, 8, 28702−28714

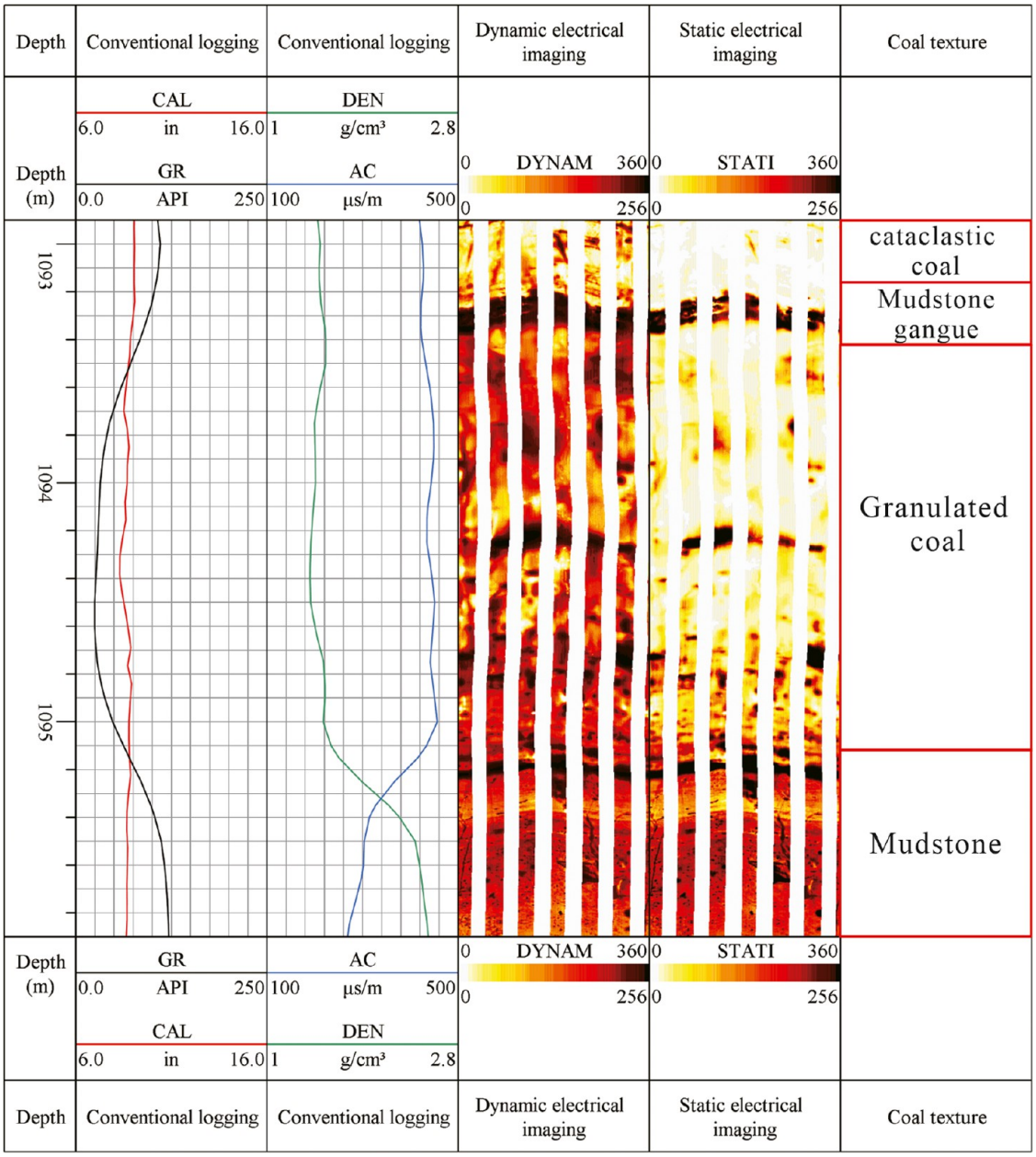

Figure 7. Electrical imaging identification map of coal texture in well CS-7 (the depth is 1092.9−1095.9 m).

characteristic value of F_2 is 11.311, with a variance of 31.4% and a typical correlation of 0.959. The cumulative variance contribution rate of functions F_1 and F_2 is 95.7%, indicating that the characteristic vectors of the characteristic values of these functions can represent the classification information of this type of function.

By inputting sample data of different coal textures into functions F_1 and F_2, the values of F_1 and F_2 for different coal textures can be obtained. By plotting these values on a two-dimensional coordinate system with F_1 as the horizontal axis and F_2 as the vertical axis, the coal texture logging interpretation chart can be obtained (Figure 10). The individual data points representing different coal textures on the chart overlap only slightly, indicating that the sample coal texture classification is effective.

If the classification result of the coal texture logging interpretation chart is not ideal or the chart cannot clearly determine the specific classification of unknown samples, the classification functions can be used. In this study, four classification functions for different coal textures were further obtained through Fisher discriminant analysis (Table 5).

The coefficients and constants of the classification functions for different coal textures are obviously different. By substituting the data of unknown samples into the classification functions represented by different coal textures and according to the principle of maximum membership degree, the function with the maximum calculated value is assigned to the corresponding coal texture classification. The classification functions for different coal textures are as follows

$$\text{undeformed} = 2294.730 \times \text{DEN} + 9.894 \times \text{AC} - 1.530 \times \text{GR} + 0.097 \times \text{RD} - 3822.519 \quad (20)$$

https://doi.org/10.1021/acsomega.3c03399
ACS Omega 2023, 8, 28702−28714

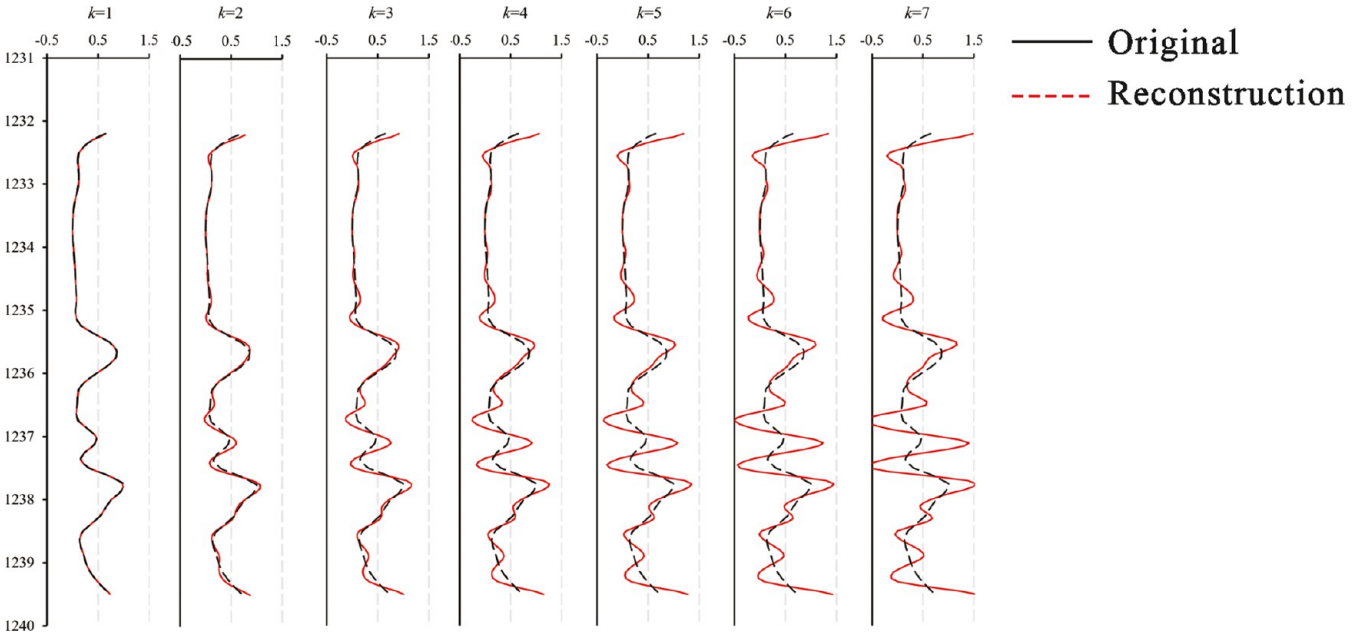

Figure 8. Schematic diagram of DEN curve reconstruction for different *k* values.

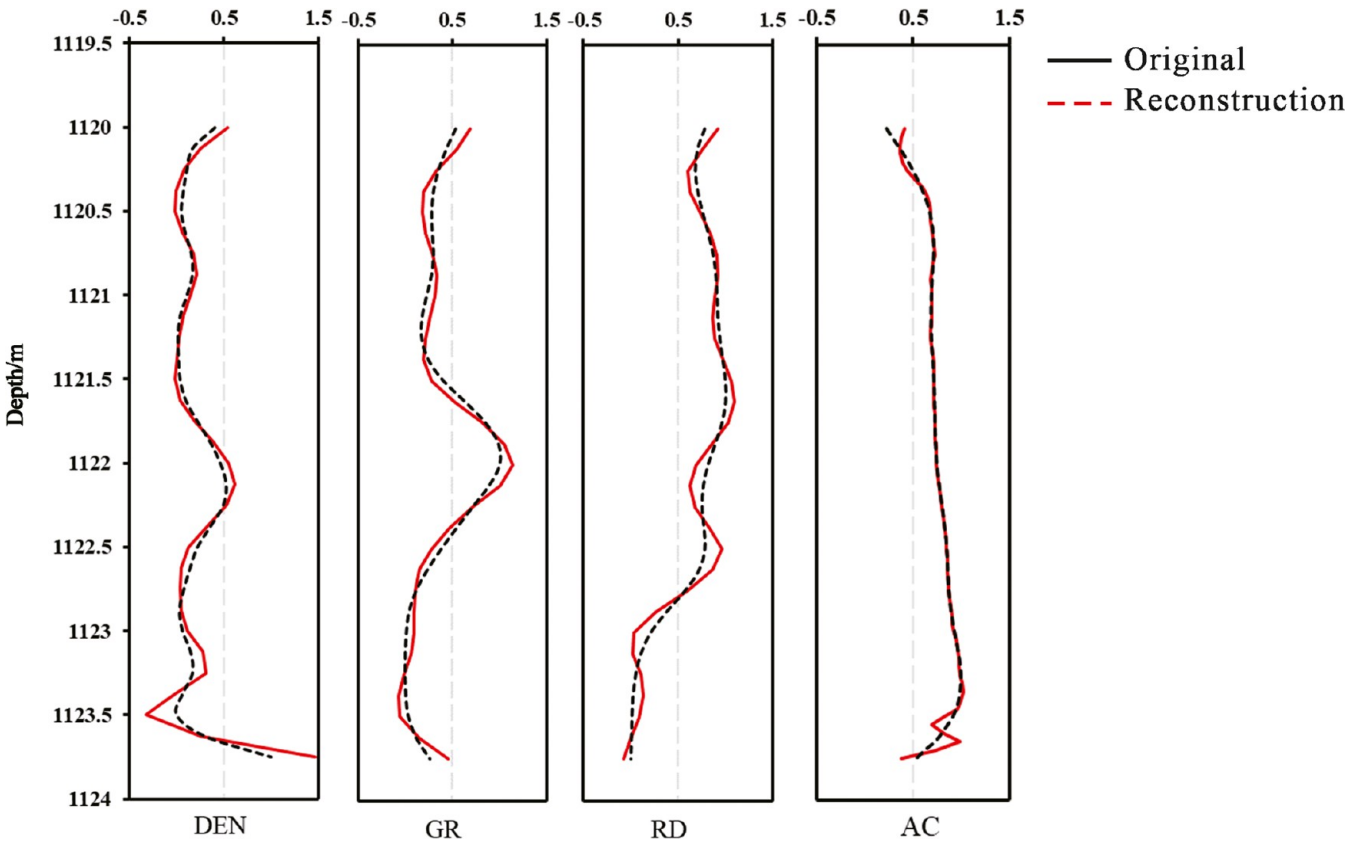

Figure 9. Schematic diagram of reconstruction curves of the No.15 coal seam in the Shouyang Block.

$$\text{cataclastic} = 2259.783 \times \text{DEN} + 9.608 \times \text{AC} - 1.474 \times \text{GR} + 0.109 \times \text{RD} - 3672.487 \quad (21)$$

$$\text{granulated} = 2374.496 \times \text{DEN} + 9.995 \times \text{AC} - 1.562 \times \text{GR} + 0.139 \times \text{RD} - 4092.448 \quad (22)$$

$$\text{gangue} = 2527.016 \times \text{DEN} + 10.01 \times \text{AC} - 1.276 \times \text{GR} + 0.109 \times \text{RD} - 4321.99 \quad (23)$$

Cross-Validation and Application. Based on the four classification functions mentioned above, the 176 sets of data used in the Fisher discriminant analysis were further substituted

https://doi.org/10.1021/acsomega.3c03399
ACS Omega 2023, 8, 28702−28714

Table 2. Statistical Result of Logging Parameters Grouped by Different Coal Textures

classification	parameters	mean value	standard deviation	number of effective cases
undeformed	DEN	1.411	0.075	59
	AC	440.776	9.570	59
	GR	37.872	21.715	59
	RD	1038.757	254.033	59
cataclastic	DEN	1.385	0.045	58
	AC	420.673	16.741	58
	GR	47.163	13.672	58
	RD	2199.849	291.569	58
granulated	DEN	1.355	0.026	48
	AC	439.038	6.874	48
	GR	32.414	9.861	48
	RD	4507.013	362.758	48
gangue	DEN	2.139	0.168	11
	AC	343.889	47.488	11
	GR	214.714	107.143	11
	RD	619.838	406.156	11
total	DEN	1.433	0.196	176
	AC	427.621	28.530	176
	GR	50.498	52.359	176
	RD	2341.095	1464.664	176

Table 3. Typical Discriminant Function Coefficient of Logging Parameters

	function	
parameter	F_1	F_2
DEN	4.3203	18.7134
AC	0.0104	0.0200
GR	−0.0068	0.0154
RD	0.0034	0.0010
constant	−18.3341	−38.3838

Table 4. Characteristic Value of Typical Discriminant Function of the No. 15 Coal Seam Texture in the Shouyang Block

function	characteristic values	variance percentage, %	cumulative percentage, %	typical correlation
F_1	23.149	64.3	64.3	0.979
F_2	11.311	31.4	95.7	0.959

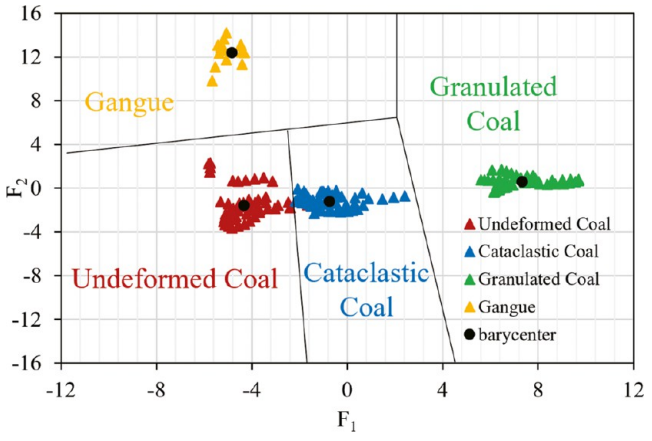

Figure 10. Interpretation chart of coal texture for the No. 15 coal seam in the Shouyang Block.

Table 5. Classification Function Coefficients of the No. 15 Coal Seam with Different Coal Texture in the Shouyang Block

	coal texture classification			
logging parameters	undeformed	cataclastic	granulated	gangue
DEN	2294.730	2259.783	2374.496	2527.016
AC	9.894	9.608	9.995	10.010
GR	−1.530	−1.474	−1.562	−1.276
RD	0.097	0.109	0.139	0.109
constant	−3822.519	−3672.487	−4092.448	−4321.99

into the above formula to obtain the discriminant classification results of the initial samples (Table 6) for cross-validation. The results show that the classification function correctly classified 99.4% of the original known cases.

By utilizing eqs 24, 25, and Table 7, it is possible to calculate the precision and recall rates for each coal texture.

$$\text{precision} = \frac{\text{TP}}{\text{TP} + \text{FP}} \tag{24}$$

$$\text{recall} = \frac{\text{TP}}{\text{TP} + \text{FN}} \tag{25}$$

where TP represents the successful prediction of a positive sample as positive, FP represents the incorrect prediction of a negative sample as positive, and FN represents the incorrect prediction of a positive sample as negative.

Equations 26 and 27 were employed to conduct a composite assessment of the individual coal texture. The macro-precision and macro-recall produced by this classification chart were both 0.996.

$$\text{macro} - \text{precision} = \frac{P_{\text{undeformed}} + P_{\text{cataclastic}} + P_{\text{granulated}} + P_{\text{gangue}}}{4} \tag{26}$$

$$\text{macro} - \text{recall} = \frac{R_{\text{undeformed}} + R_{\text{cataclastic}} + R_{\text{granulated}} + R_{\text{gangue}}}{4} \tag{27}$$

To further verify the practicality of the coal texture logging interpretation method mentioned above, interpretation analyses were performed on the No. 15 coal seam of CS-8 and CS-9 wells, and the results were compared with the core description results obtained on site. The well logging parameters of these two wells are not involved in the model building phase and are representative. As shown in the core photos corrected by electrical imaging logging in Figure 11, the coal textures of the No. 15 coal seam in the CS-8 well from top to bottom are cataclastic coal and undeformed coal, while in CS-9 well, the coal textures are recognized as undeformed coal, cataclastic coal, granulated coal, cataclastic coal, and undeformed coal, respectively, with argillaceous gangue (mudstone) developing inside the undeformed coal at the bottom.

Figures 12 and 13 show the projection of the logging data at different depths on the coal texture discrimination chart for these two wells. Based on the recognition of the discrimination map and the calculation results of the classification function, the coal texture of the No. 15 coal seam in the CS-8 well was divided. Only one point representing cataclastic coal identified by the core falls into the granulated coal area on the chart and one point

https://doi.org/10.1021/acsomega.3c03399
ACS Omega 2023, 8, 28702−28714

Table 6. Classification Results of Coal Texture of the No. 15 Coal Seam in the Shouyang Block

			prediction results				
	classification		undeformed	cataclastic	granulated	gangue	total
original	sample	undeformed	59	0	0	0	59
		cataclastic	0	58	0	0	58
		granulated	0	0	48	0	48
		gangue	0	0	0	11	11
	percentage, %	undeformed	100	0	0	0	100
		cataclastic	0	100	0	0	100
		granulated	0	0	100	0	100
		gangue	0	0	0	100	100
cross-validation	sample	undeformed	58	1	0	0	59
		cataclastic	0	58	0	0	58
		granulated	0	0	48	0	48
		gangue	0	0	0	11	11
	percentage, %	undeformed	98.3	1.7	0	0	100
		cataclastic	0	100	0	0	100
		granulated	0	0	100	0	100
		gangue	0	0	0	100	100

Table 7. Statistical Table of TP, FN, and FP of the Coal Body Structure

		TP	FN	FP
classification	undeformed	58	1	0
	cataclastic	58	0	1
	granulated	48	0	0
	gangue	11	0	0

representing undeformed coal falls into the gangue area, indicating an accuracy rate of 97.1% when compared with the core identification results. For the No. 15 coal seam in CS-9 well, two points representing cataclastic coal falls into the granulated coal area, and only one point representing undeformed coal falls into the cataclastic coal area. Moreover, a point representing gangue and a point representing cataclastic coal fall into the undeformed coal area, resulting in an accuracy rate of 93.2%, and its macro-precision and macro-recall values are 0.919 and 0.916, respectively. Therefore, the established coal texture identification chart and classification function can be effectively applied to predict and analyze unknown samples.

CONCLUSIONS

This study systematically establishes a coal texture interpretation method, including core depth correction, core repositioning, coal texture correction, wavelet transformation (decomposition and reconstruction), Fisher discriminant analysis, determination of the classification function, and the establishment of the coal texture logging interpretation chart. This method effectively improves the vertical resolution of logging curves and the accuracy of coal texture prediction.

The wavelet decomposition and reconstruction method can preserve the effective information of thick layers without distortion while magnifying the information of thin layers and eliminating noise. In the wavelet reconstruction formula for the No. 15 coal seam in the Shouyang Block, $k = 3$ is selected as the compensation coefficient for the deep resistivity curve, $k = 4$ as the compensation coefficient for the density and sonic time difference curve, and $k = 7$ as the compensation coefficient for the natural γ curve.

Using Fisher discriminant analysis, a coal texture discrimination chart for the No. 15 coal seam in the Shouyang Block is established. The classification accuracy is 99.4%, and it can effectively distinguish undeformed coal, cataclastic coal, granulated coal, and gangue. The effectiveness of the chart is verified using the No. 15 coal seam in wells of CS-8 and CS-9, with accuracy rates of 97.1 and 93.2%, respectively. Overall, the built coal texture logging interpretation chart and classification function through Fisher discriminant analysis can be effectively applied to the precise prediction of coal textures.

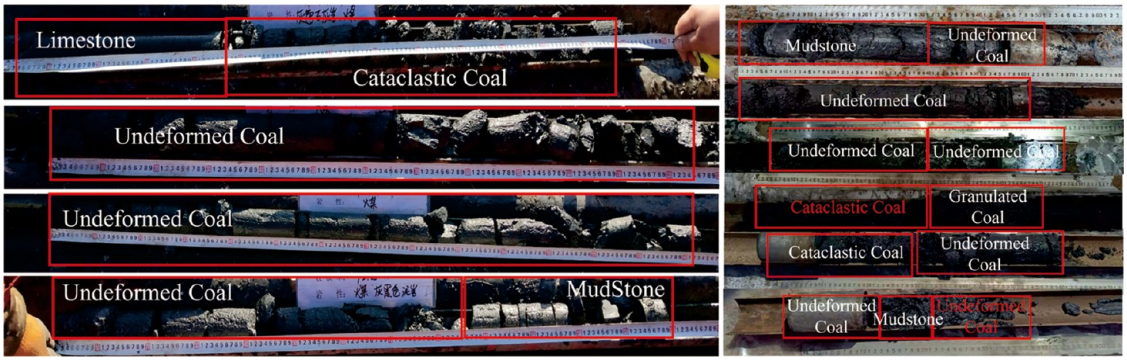

Figure 11. Verification of coal structural identification results with core photos of CS-8 (left) and CS-9 (right).

https://doi.org/10.1021/acsomega.3c03399
ACS Omega 2023, 8, 28702−28714

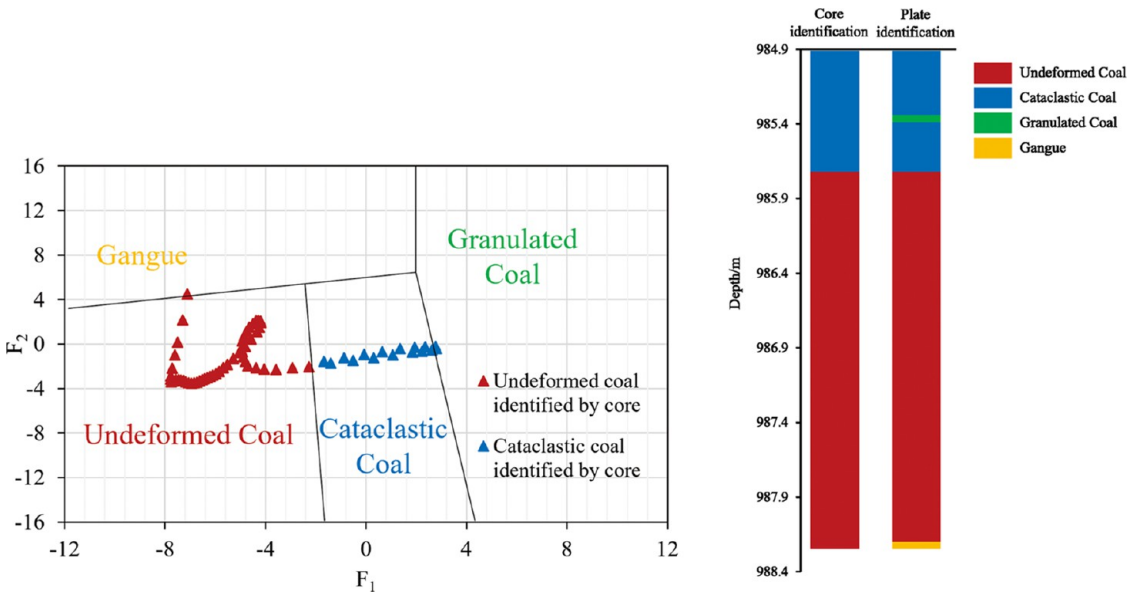

Figure 12. Projection discrimination of coal texture of the No. 15 coal seam of well CS-8 and its comparison with core discrimination results (the chart is the same as Figure 10).

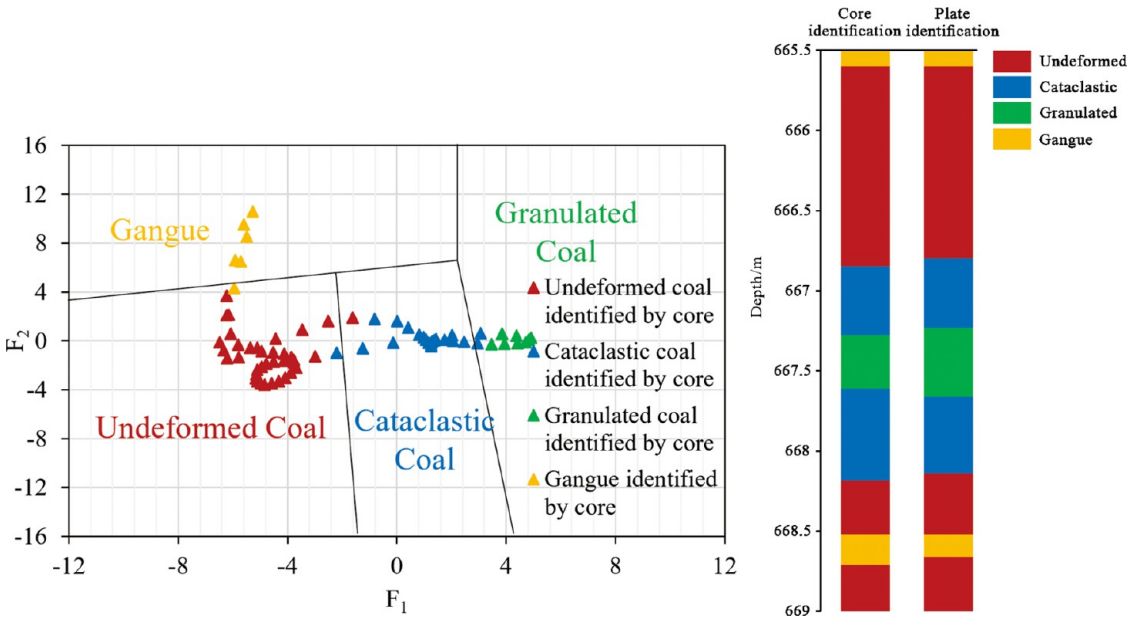

Figure 13. Projection discrimination of coal texture of the No. 15 coal seam of well CS-9 and its comparison with core discrimination results (the chart is the same as Figure 10).

AUTHOR INFORMATION

Corresponding Author

Shouren Zhang − *China United Coalbed Methane Corporation Ltd., Beijing 100015, China;* orcid.org/0009-0002-4396-9279; Email: zhonglianshangsr@163.com

Authors

Xinyang Men − *School of Energy Resources, China University of Geosciences (Beijing), Beijing 100083, China*

Zhiyu Deng − *China United Coalbed Methane Corporation Ltd., Beijing 100015, China*

Qiuping Hu − *China United Coalbed Methane Corporation Ltd., Beijing 100015, China*

Complete contact information is available at: https://pubs.acs.org/10.1021/acsomega.3c03399

Notes

The authors declare no competing financial interest.

ACKNOWLEDGMENTS

This work was supported by the China United Coalbed Methane Co., Ltd. Seven-Year Action Plan Technology Project: Research on Coalbed Methane Storage and Transportation Technology (CNOOC-KJ135ZDXM 40 ZL01). The authors would like to be grateful to the editor and anonymous reviewers for their careful reviews and detailed comments, which helped to substantially improve the manuscript.

REFERENCES

(1) Wang, E. Y.; Liu, M. J.; Wei, J. P. New genetic−texture−structure classification system of tectonic coal. *J. China Coal Soc.* **2009**, *34*, 656−660.

(2) Guo, G. S.; et al. Comprehensive evaluation of coal rock quality based on "three structures" of coal seam. *China Offshore Oil Gas* **2022**, *34*, 35−41.

(3) Ma, T. S.; Liu, J. H.; Fu, J. H.; Wu, B. S. Drilling and completion technologies of coalbed methane exploitation: an overview. *Int. J. Coal Sci. Technol.* **2022**, *9*, 68−98.

(4) Zhang, J. G.; Han, S.; Zhang, C.; Chen, Y. J. Coal structure identification by logging based on coal accumulation environment zoning and its application in Mabidong Block, Qinshui Basin. *Coal Geol. Explor.* **2021**, *49*, 114−122.

(5) Fu, X. H.; Lu, G. Z.; Qin, J.; Jia, H. Y. Determination of coalbed gas content and classification of coal structure with log response. *Well Logging Technol.* **1999**, *2*, 112−115.

(6) Hu, G. Q.; Jiang, B.; Chen, F.; Qu, Z. H. Study on different type structure coal features and gas outburst control. *Coal Sci. Technol.* **2012**, *2*, 111−115.

(7) Yao, J. P.; SiMa, L. Q.; Zhang, Y. G. Quantitative identification of deformed coals by geophysical logging. *J. China Coal Soc.* **2011**, *36*, 94−98.

(8) Li, L. J.; Liu, D. M.; Cai, Y. D.; Wang, Y. J.; Jia, Q. F. Coal structure and its implications for coalbed methane exploitation: a review. *Energy Fuels* **2021**, *35*, 86−110.

(9) Ai, L.; Zhou, M. S.; Zhang, J.; Liang, X.; Qian, B. W.; Liu, D. R. Quantitative identification of coal structure based on coal rock brittleness index by logging data. *Lithol. Reserv.* **2017**, *29*, 139−144.

(10) Li, J. T.; Wang, R. J.; Gao, B.; Wu, C. F.; et al. Characteristics of coal structure and construction of well logging model in Baoan block of Xinjing Mine. *Min. Saf. Environ. Prot.* **2022**, *15*, 72−77.

(11) Li, C. L.; Yang, Z. B.; Sun, H. S.; Ma, Y. Y.; Zhang, Z. G.; Li, Y. Y.; Li, G. Construction of a logging interpretation model for coal structure from multi-coal seams area. *J. China Coal Soc.* **2020**, *45*, 721−730.

(12) Zhang, Z.; Qin, Y.; Wang, G.; Sun, H.; You, Z.; Jin, J.; Yang, Z. Evaluation of coal body structures and their distributions by geophysical logging methods: case study in the Laochang block, eastern Yunnan, China. *Nat. Resour. Res.* **2021**, *30*, 2225−2239.

(13) Li, C.; Yang, Z.; Tian, W.; Lu, B. Construction and application of prediction methods for coal texture of CBM reservoirs at the block scale. *J. Pet. Sci. Eng.* **2022**, *219*, No. 111075.

(14) Shu, Y.; Sang, S.; Zhou, X.; Zhao, F. Coal Body Structure Detection Based on Logging and Seismic Data and Its Impacts on Coalbed Methane Development: A Case Study in the Dahebian Block, Western Guizhou, Southern China. *Nat. Resour. Res.* **2023**, *32*, 691−716.

(15) Chen, S. D.; Liu, P. C.; Tang, D. Z.; Tao, S.; Zhang, T. Y. Identification of thin-layer coal texture using geophysical logging data: Investigation by wavelet transform and linear discrimination analysis. *Int. J. Coal Geol.* **2021**, *239*, No. 103727.

(16) Wang, L.; Shen, J. S.; Heng, H. L.; Wei, S. S. Automatic fractured-vuggy identification and extraction from electric imaging logging data based on an incomplete path opening operation and a sinusoidal database. *Pet. Sci. Bull.* **2021**, *03*, 380−395.

(17) Tao, S.; Tang, D. Z.; Xu, H.; Gao, L. J.; Fang, Y. Factors controlling high-yield coalbed methane vertical wells in the Fanzhuang Block, southern Qinshui Basin. *Int. J. Coal Geol.* **2014**, *134−135*, 38−45.

(18) Zhao, J. L.; Tang, D. Z.; Qin, Y.; Xu, H. Experimental study on structural models of coal macrolithotypes and its well logging responses in the Hancheng area, Ordos Basin, China. *J. Pet. Sci. Eng.* **2018**, *166*, 658−672.

(19) Tao, S.; Pan, Z. J.; Tang, S. L.; Chen, S. D. Current status and geological conditions for the applicability of CBM drilling technologies in China: A review. *Int. J. Coal Geol.* **2019**, *202*, 95−108.

(20) Duan, H. Y.; Duan, H. F.; Xie, W. D. Recognition of coal structure based on different logging curves: Case study of Tashan mine in Datong coalfield. *J. Henan Polytechnic Univ. (Nat. Sci.)* **2021**, *40*, 59−65.

(21) Basso, M.; Souza, J. P. P.; Honório, B. C. Z.; Melani, L. H.; Chinelatto, G. F.; Belila, A. M. P.; Vidal, A. C. Acoustic image log facies and well log petrophysical evaluation of the Barra Velha Formation carbonate reservoir from the Santos Basin, offshore Brazil. *Carbonates Evaporites* **2022**, *37*, 50.

(22) Liu, J.; Wang, J.; Fu, Q.; Tan, Q. S.; Sun, D. M. Study on logging response characteristics and distribution of coal rock structure in Zheng-zhuang Area. *China Coalbed Methane* **2013**, *10*, 9−14.

(23) Zhai, L. L.; Wang, L. T. Numerical inversion methods for enhancing well logging resolving power. *Basic Sci. J. Text. Univ.* **2015**, *28*, 243−247.

(24) Kadkhodaie, A.; Rezaee, R. Intelligent sequence stratigraphy through a wavelet-based decomposition of well log data. *J. Nat. Gas Sci. Eng.* **2017**, *40*, 38−50.

(25) Maiti, S.; Tiwari, R. K. Automatic detection of lithologic boundaries using the Walsh transform: A case study from the KTB borehole. *Comput. Geosci.* **2005**, *31*, 949−955.

(26) Giles, P. S. Time Series Analysis and Cyclostratigraphy: Examining stratigraphic records of environmental cycles. *Geosci. Canada* **2006**, *33*, 32−33.

(27) Chada, N. K.; Stuart, A. M.; Tong, X. T. Tikhonov regularization within ensemble Kalman inversion. *SIAM J. Numer. Anal.* **2020**, *58*, 1263−1294.

(28) Bolton, E. W.; Maasch, K. A.; Lilly, J. M. A wavelet analysis of Plio-Pleistocene climate indicators: A new view of periodicity evolution. *Geophys. Res. Lett.* **1995**, *22*, 2753−2756.

(29) Yu, S.; Jiang, B.; Li, M.; Hou, C. L.; Xu, S. C. A review on pore-fractures in tectonically deformed coals. *Fuel* **2020**, *278*, No. 118248.

(30) Liao, G. Z.; Li, Y. Z.; Xiao, L. Z.; Qin, Z. J.; Hu, X. Y.; Hu, F. L. Prediction of microscopic pore structure of tight reservoirs using convolutional neural network model. *Pet. Sci. Bull.* **2020**, 26−38.

(31) Zou, G. G.; Zhang, Q. H.; Peng, S. P.; She, J. H.; Teng, D. L.; Jin, C. C.; Che, Y. Y. Influence of geological factors on coal permeability in the Sihe coal mine. *Int. J. Coal Sci. Technol.* **2022**, *9*, 6−18.

(32) Gong, Y.; Jia, R. S.; Lu, X. M.; Peng, Y. J.; Zhao, W. D.; Zhang, X. L. To suppress the random noise in microseismic signal by using empirical mode decomposition and wavelet transform. *J. China Coal Soc.* **2018**, *43*, 3247−3256.

https://doi.org/10.1021/acsomega.3c03399
ACS Omega 2023, 8, 28702−28714